



Liquefiable Concrete Tunnel–Sand–Pile Interaction Response Under Seismic Excitations

Md. Faisal Haque · Mehedi Ahmed Ansary

Received: 13 April 2023 / Accepted: 20 July 2023 / Published online: 28 July 2023
© The Author(s), under exclusive licence to Springer Nature Switzerland AG 2023

Abstract This paper presents the concrete tunnel-sand-pile interaction (TSPI) phenomenon in liquefiable sand considering various relative densities and seismic excitations. The novel shake table test for the TSPI model was performed to evaluate the excess pore pressure ratio (EPPR) surrounding the tunnel body and interactive tunnel and pile moments. The relative densities are taken to be 27, 41, and 55% in the local sand of Bangladesh. Similarly, the peak ground acceleration (PGA) of the Kobe and Loma Prieta earthquakes are considered to be 0.05, 0.10, 0.15, and 0.20 g. The shake table was calibrated based on similar variations of the input and output PGA. The 3D finite element concrete TSPI model has been performed by Plaxis considering the UBC3D-PLM (two yield surfaces consisting of kinematic hardening rules) constitutive model of sand. Therefore, experimental and numerical results vary closely, which may inform the possibility of the application of the concrete TSPI model on a large scale. The maximum SRSS (Square Root Sum of Squares) tunnel moment has been found to be 18.7 kN-m from the experimental results for 27% relative density of the Kobe earthquake with a PGA of 0.15 g. Also, the

maximum SRSS moments of front and rear piles vary (0.10–0.14) % of the tunnel moment. So, the tunnel moment always shows a higher value in liquefiable ground based on the experimental results because of the larger volume and stiffness than a series of piles. However, the present study may be enhanced in the future by varying geometric properties.

Keywords Excess pore pressure ratio · Interactive moments · Seismic excitations · Tunnel–Sand–Pile Interaction · UBC3D-PLM

1 Introduction

The study of the liquefiable tunnel-sand-pile interaction (TSPI) response is an innovative technique under seismic excitations. Recently, some studies (Taylor and Madabhushi 2020; Zhao et al. 2021; Orang et al. 2021; Yue et al. 2021; Hussein and Naggar 2021; Wang et al. 2022) have been completed to consider the liquefaction impact on the tunnel-soil or pile-soil interactions. From that point of view, the present study is logical to evaluate the seismic TSPI liquefiable response. However, liquefaction is a common phenomenon during seismic excitation having the capability to hamper underground structures (e.g. tunnels, piles, etc.). For example, the pile resistance was diminished for the fully liquefied state of the soil (Hussein and Naggar 2021). Also, the moment of the box tunnel was found to be 475 kN–m/m

M. F. Haque (✉) · M. A. Ansary
Department of Civil Engineering, Bangladesh University
of Engineering and Technology, Dhaka 1000, Bangladesh
e-mail: mfh.civil@gmail.com

M. A. Ansary
e-mail: ansaryma66@gmail.com

from the centrifugal test at a certain period of seismic excitation due to the occurrence of liquefaction (Wang et al. 2022). So, experimental and numerical studies inform some ideas about the impact of liquefaction on the tunnel and pile structures at some specific locations. Although, it is very difficult to predict liquefaction impact on the whole length of the tunnel body theoretically and experimentally with the presence of piles. This information can help the designer for understanding the liquefiable interactive response of the tunnel with the presence of piles or vice-versa. Therefore, the present study performs the experimental shake table test and numerical analysis to predict the interactive responses of the tunnel and pile due to the existence of liquefaction under seismic excitations.

Recently, the shake table test of a horseshoe and circular tunnels was completed under seismic excitation (Taylor and Madabhushi 2020; Yue et al. 2021). The diameter of the circular tunnel was used to be 500 mm which was 4 m on a large (prototype) scale (Yue et al. 2021). So, the scale factor was 8. In both tunnels (circular and horseshoe), the cover-to-diameter ratio was maintained to be 0.38. Also, the cover-to-diameter ratio was used to be 0.65 for the box tunnel (Wang et al. 2022). However, concrete TSPI is scarce in the literature, although many kinds of research have been already completed for the only tunnel (Taylor and Madabhushi 2020; Zhao et al. 2020; Zhao et al. 2021; Yue et al. 2021) and pile (Finn and Fujita 2002; Bhattacharya et al. 2004; Maheshwari et al. 2008; Hussein and Naggat 2021; Tang et al. 2021; Orang et al. 2021; Huded et al. 2022; Sahare et al. 2022) under the uniform sinusoidal wave and non-uniform seismic excitations. In reality, many tunnels are passed through the adjacent pile in the urban area of the world. But existing works of literature are unable to express the TSPI response because of the lackings of experimental and numerical studies. Although it was given some basic idea about tunnels and piles under liquefiable conditions. In a recent study excluding piles, displacements of the tunnel were more fluctuated due to the existence of liquefaction (Yue et al. 2021). The most recent study described the response of the TSPI model numerically due to the existence of liquefaction (Haque 2023). According to that study, liquefaction potential slightly increased with the addition of a series of piles along the length of the tunnel. Also, it was

evaluated that the impact of piles on the tunnel body was very less because of less volume and weight of piles compare to the tunnel. For those reasons, previous researchers may not be included piles in their analysis to avoid complexity. However, geometric configurations of the present model are decided based on previous works of literature for the tunnel or pile only. Recent works of literature are listed in Table 1. In the present study, the tunnel diameter is taken to be 4 m (prototype) because of maintaining other dimensions of the TSPI model. In addition, the tunnel diameter of the 1:20 scale of this study is the same as the diameter of the 1:8 scale of the previous study (Yue et al. 2021). Another important term of this study is the selection of seismic excitation. Seismic excitation is selected based on the liquefaction history. The two historic earthquakes of Kobe and Loma Prieta carried significant damage to soil and structure due to liquefaction. At that time these earthquakes significantly hampered life-line structures because of the lackings of design codes, formulations, material models, etc. By the way, a numerical study (Bao et al. 2017) of a large metro subway tunnel was completed to consider the Kobe earthquake record for the evaluation of the interactive responses of the tunnel due to the existence of liquefaction. Based on these reasons, the present research considers the two historic seismic records. Six recent large earthquake records are listed in Table 2 to consider peak ground acceleration because of hampering significant areas by induced liquefaction during those earthquakes. In Table 2, peak ground accelerations were recorded to be 0.47 g and 0.25 g for Haiti (14 August 2021) and Nepal (25 April 2015) earthquakes, respectively. In the present research, the selection of peak ground accelerations of two historic earthquakes are stand within the range of recent larger earthquakes. Other issues are pile diameter and length. For the mitigation of the building settlements due to the liquefaction, a large-scale shake table test was performed in the laboratory considering a helical pile with a diameter of 200 mm (Orang et al. 2021). The pile diameter in the prototype scale is taken to be 300 mm in this study considering the 4-storied building load on the pile cap. Similarly, pile cap dimension and the length of the pile are considered based on this building load, soil conditions, clearance of the tunnel and pile, etc. In the most recent study, the pile deflection was predicted larger due to liquefaction compared to the non-liquefiable

Table 1 Summary of soil, pile, tunnel, and excess pore pressure ratio from previously published works

SL No	Reference	Soil Parameters		Pile Parameters		Tunnel Parameters			EPWR ⁱ
		C ⁱⁱ (kPa)	ϕ ⁱⁱⁱ (°)	^{iv} D _p (mm)	^v L _p (m)	^{vi} D _T (m)	Cover to Dia. Ratio	Type	
1	Bhattacharya et al. (2004)	/	32	9.3	0.160	/ ^{vii}	/	/	1.4
2	Wang et al. (2022)	/	/	/	/	8.8	0.65	Box	1.1
3	Zhao et al. (2021)	0	30	/	/	14.3	0.15	Double Box	1.3
4	Taylor and Madabhushi (2020)	/	/	/	/	0.13	0.38	Horse Shoe	1.1
5	Orang et al. (2021)	/	35	200	2.2	/	/	/	> 1
6	Yue et al. (2021)	/	27.9	/	/	0.5	0.38	Circular	1.1
7	Hussein and Naggar (2021)	/	37.5	0.10	1.65	/	/	/	1.2

SL No	Reference	Displacements			Lateral Tunnel Moment (kNm/m)	Peak Acceleration (in terms of “g”)	Study Type
		Soil Vertical (mm)	Pile Lateral (mm)	Tunnel Lateral (mm)			
1	Bhattacharya et al. (2004)	/	/	/	/	1.00	Dynamic Centrifuge Test (1:50)
2	Wang et al. (2022)	0.20	/	/	475	0.67	Centrifuge Test
3	Zhao et al. (2021)	/	/	/	/	0.30	Calibrated Numerical Model
4	Taylor and Madabhushi (2020)	/	/	/	/	0.60	Shake Table Test (Model)
5	Orang et al. (2021)	440	/	/	/	0.66	Shake Table Test (Large)
6	Yue et al. (2021)	/	/	/	/	0.80	Shake Table Test (Model)
7	Hussein and Naggar (2021)	/	/	/	/	0.30	Shake Table Test (Model)

³ⁱEPWR = Excess Pore Water Ratio (e.g. EPWR ≥ 1, layer liquefied; EPWR < 1, layer non-liquefied)

ⁱⁱC = Cohesion of soil

ⁱⁱⁱ ϕ = Angle of internal friction

^{iv}D_p = Pile diameter

^vL_p = Pile Length

^{vi}D_T = Tunnel Diameter

^{vii}/ = Not Found

medium because of heavy losses of strength and stiffness of the surrounding soil medium (Huded et al. 2022). However, soil losses its shear strength due to the occurrence of liquefaction which causes sudden changes in the adjacent structures in the soil medium. For the gradual eruption of sand boils due to the liquefaction, sand losses frictional resistance and intermolecular attractive forces. For this reason, tunnels and adjacent structures may be more hampered due to the liquefaction phenomenon. Therefore, this study records the impact of the liquefaction on the tunnel and pile bodies although it is very difficult to evaluate this impact practically. However, liquefaction in terms

of effective stress was measured by the build-up of excess pore pressure inside the soil mass which happened at several depths of the soil layer (Liyanapathirana and Poulos 2002). Liquefaction was evaluated in terms of excess pore pressure ratio (EPPR) for the prediction of the seismic performances of the steel utility tunnel using the shake table test (Yue et al. 2021). EPPR was related to effective vertical stress. Liquefaction existed when EPPR exceeded the unit value based on the previous study of the steel utility tunnel. According to those studies, liquefaction is estimated in the present study in terms of the excess pore pressure ratio.

Table 2 Largest earthquakes histories of last twelve years

SL No	Date	Place	Epicenter Location	Lowest Epicentral Distance (km)	Focal Depth (km)	Intensity and Damage State	Moment Magnitude (USGS)	Casualties	Peak Acceleration	Fault	Type	Estimated Total Damage Cost (USD)	Liquefaction History
1	6 Feb. 2023	Turkey and Syria	37.166°N 37.032°E	27	17.9	XI (Extreme)	7.8	43,850+deaths and 120,000 injured	1.62 g	East Anatolian	Strike-Slip	84.1 billion	Significant Area Affected
2	22 June 2022	Afghanistan	33.02°N 69.46°E	55	4	VIII (Severe)	6.2	1163 deaths and 6027+injured	/	/	Strike-Slip	/	Little/No Area Affected
3	14 Aug. 2021	Haiti	18.417°N 73.480°W	0	10	VIII (Severe)	7.2	2248 deaths and 12,763 injured	0.47 g	Enriquillo-Plantain Garden	Oblique-Reverse	1.5–1.7 billion	Significant Area Affected
4	28 Sep. 2018	Indonesia	0.178°S 119.840°E	72	20	X (Extreme)	7.5	4340 deaths and 10,679 injured	1.54 g	Palu-Koro	Strike-Slip	/	Significant Area Affected
5	25 April 2015	Nepal	28.230°N 84.731°E	67	8.2	X (Extreme)	7.8	8964 deaths and 21,952 injured	0.25 g	Main Himalayan Thrust	Thrust	/	Extensive Area Affected
6	11 March 2011	Japan	38.322°N 142.369°E	Tsunami	29	IX (Violent)	9.1	19,759 deaths and 6242 injured	2.99 g	Tsunami	Mega Thrust	360 billion	Extensive Area Affected

The main objective of the present study is the developing the TSPI model using the shake table for evaluating the interactive responses of the tunnel and pile in the liquefiable ground under seismic excitations. Scaled Kobe and Loma Prieta seismic excitations are applied at the bottom of the model along the transverse direction of the tunnel because the lateral movement of the tunnel is more crucial than longitudinal movement. Peak ground accelerations of both excitations are taken to be 5%, 10%, 15%, and 20% of the corresponding gravitational acceleration because of the prediction of the variations of the tunnel and pile moments in different liquefiable ground conditions to achieve the goal of this study. Responses of the tunnel, pile, and excess pore pressure ratio of the soil are recorded for various relative densities of sand because of variations of the radiation damping depending on the soil stiffness linked to the relative density. In this study, geometric properties are constant because of avoiding complexity for this complex interaction model, and material properties are taken from the laboratory test. Relative densities, peak ground accelerations, and seismic excitations are the three variable parameters of this study to evaluate the interactive response of the TSPI model. The shake table is calibrated and experimental results are compared with the numerical analysis for improving the accuracy of this study.

2 Experimental Investigation

Firstly, conducted the experimental work of the TSPI model. The experimental setup was performed by maintaining some steps. Therefore, these schematic steps are discussed herein.

Step-1 Stone chips, fine sand, cement, and weir mesh were collected to perform the test whose properties were known from either the standard specification or laboratory test.

Step-2 Shuttering materials of plastic pipe, plywood, connecting screws, etc. were prepared by maintaining the proper size and shape of the tunnel, pile, and pile cap before casting.

Step-3 Tunnel, pile, and pile cap was cast on the same day.

Step-4 Casted samples of tunnel, pile, and pile cap were cured in the laboratory for 28 days.

Step-5 Compressive strength tests of 28 days cured cubical samples of tunnel and pile were conducted in the laboratory.

Step-6 The thin polythene layer was placed inside the laminar box on the shake table.

Step-7 A sand bed was prepared for the specific relative density by the Pluviator technique.

Step-8 The tunnel and piles along with caps were placed inside the laminar box at a certain level using the mechanical crane.

Step-9 Pore pressures and strain gauges were placed at a specific location of the TSPI model.

Step-10 Scaled Kobe and Loma Prieta seismic excitations were applied along the transverse direction of the tunnel using the input computer in the control room of the laboratory.

Step-11 Finally, output data were recorded on the laptop.

2.1 Equipment of Experimental Test

For the availability of the concrete laboratory in BUET (Bangladesh University of Engineering and Technology), we used a 1 g and 1D shake table, and a steel laminar box with proper arrangements on the shake table. Many researchers (Hussein and Naggar 2021; Orang et al. 2021; Yue et al. 2021; Wang et al. 2022) used individual tunnel and pile to prepare experimental arrangements for their research. Materials of the tunnel and piles were used to be concrete in those research. Those researchers used scale factors for modeling by considering some probable factors of limitations of the laboratory to prepare the model, practical applicability of the model in the future on a large scale, etc. However, no research is found to consider tunnel and pile together for the experimental modeling by using a shake table. For this reason, the present research considers the concrete tunnel and piles along with caps for the experimental modeling by using a shake table having a reasonable scale factor of 20 (twenty). If the scale factor is less than 20 then it is not possible to maintain a reliable tunnel diameter corresponding to pile and pile cap dimensions. On the other hand, if it is greater than 20 then it is not possible to set up our 2 m × 2 m dimension shake table. Therefore, the presently used scale factor of this study may be suitable to express practical situations of the TSPI model on a large scale corresponding to tunnel and other parameter dimensions

considering all issues. Another important term is a similitude for large-scale numerical analysis. Iai (1989) proposed similitude for shaking table tests on the soil-structure-fluid model in a 1 g gravitational field considering pile structures. In that research, similitude was applied for liquefaction considering the special case of taking an apparent density scale factor of one. In the present research, similitude (Table 3) is considered based on that study (Iai 1989) because of considering liquefaction impact on the tunnel and pile of 1 g gravitational field shake table test. Tunnel, pile, pile cap, and sand are the main equipment of the present shake table test. The shake table is connected by the actuator. The movement of the actuator is controlled by the two servo valves. These valves are connected to the servo-controlled machine and this machine is controlled by the computer. Seismic or uniform excitation is input in the software of the controlling computer and induced motion hit the shake table by the actuator. For the calibration purpose of the shake table, base acceleration was measured by the accelerometer. The base accelerometer was connected to the data acquisition laptop by using the sensor-controlling device. Various pore pressure transducers and strain gauges of the TSPI model were connected to that device. During the start of the servo-controlled machine, low pressure applies first then high pressure. The value of high pressure fluctuates within a range of (21–24) MPa in most cases. The maximum range of the shake table is ± 2 g. A laminar box was attached to the shake table in the center by nuts and bolts. The outer and inner dimensions of the laminar box were measured to be 915 mm \times 1220 mm \times 1220 mm and 815 mm \times 1120 mm \times 1120 mm, respectively. The laminar box was manufactured in the laboratory and it was made of 20

hollow aluminum layers by maintaining a certain gap between successive layers in Fig. 1c. The size of the hollow aluminum bar was maintained to be 50 mm \times 50 mm \times 1.5 mm. The inside dimension of the single-layer laminar box is 815 mm \times 1120 mm \times 50 mm. During the construction of the laminar box, the ball bearing was used in the four corners of the laminar box with a diameter of 16 mm. In each layer, 12 rotating ball bearing was used, and a 2 mm thick rubber membrane protected the ball bearings. The Laminar box ensures the continuation of the adjacent layers. A solid aluminum plate was placed at the bottom of the laminar box with a size of 815 mm \times 1120 mm \times 15 mm. It ensures a fixed boundary at the bottom. In addition, the laminar box ensures a flexible boundary surrounding the inside soil of the laminar box. Inside the laminar box was wrapped by thin polythene to protect the overpass of soil into the gap of the two adjacent hollow aluminum bars. The thin polythene increases the lateral stiffness of the inside soil of the laminar box. Seismic excitation was applied along the length of the laminar box. The geometry of the shake table along with the laminar box including the direction of the input seismic excitation is shown in Fig. 1c. This paper uses the tunnel diameter of 200 mm in the TSPI model assuming small vehicle/rail movement inside the tunnel. The self-weight and moving load of small vehicles/rail are neglected from modeling/analysis because of to avoid complexity. The present study's tunnel diameter is close to the previous (Taylor and Madabhushi 2020) similar type study's tunnel diameter of 150 mm. Details geometry of the TSPI model and section (a–a) are shown in Fig. 1a and b, respectively. Pore pressure transducers and strain gauges were placed in several locations in the TSPI model to represent in Fig. 1b. These locations of sensors are selected in this research because of the evaluation of interactive responses of the tunnel and pile in the interaction zone. Liquefaction was estimated in terms of excess pore pressure ratio (EPPR). The EPPR is the function of the change in pore pressure and initial effective vertical stress which is represented in Eq. (1). Similarly, tunnel and pile moments are calculated by using Eq. (2). For the determination of the pore pressure and strain, three pore pressure transducers (P1, P2, and P3) and strain gauges (S1, S2, and S3) were placed in the TSPI model in Fig. 1b. The tunnel was prepared by using 3 mm downgraded stone chips to maintain a maxing

Table 3 Similitude of the TSPI model (P=Prototype; M=Model; scale factor= λ)

Items	P/M	M/P
Geometry and stress	λ	$1/\lambda$
Density and acceleration	1	1
Strain	$\lambda^{0.5}$	$1/\lambda^{0.5}$
Time	$\lambda^{0.75}$	$1/\lambda^{0.75}$
Moment	λ^3	$1/\lambda^3$
Frequency	$1/\lambda^{0.75}$	$\lambda^{0.75}$
Excess pore pressure ratio (EPPR)	1	1

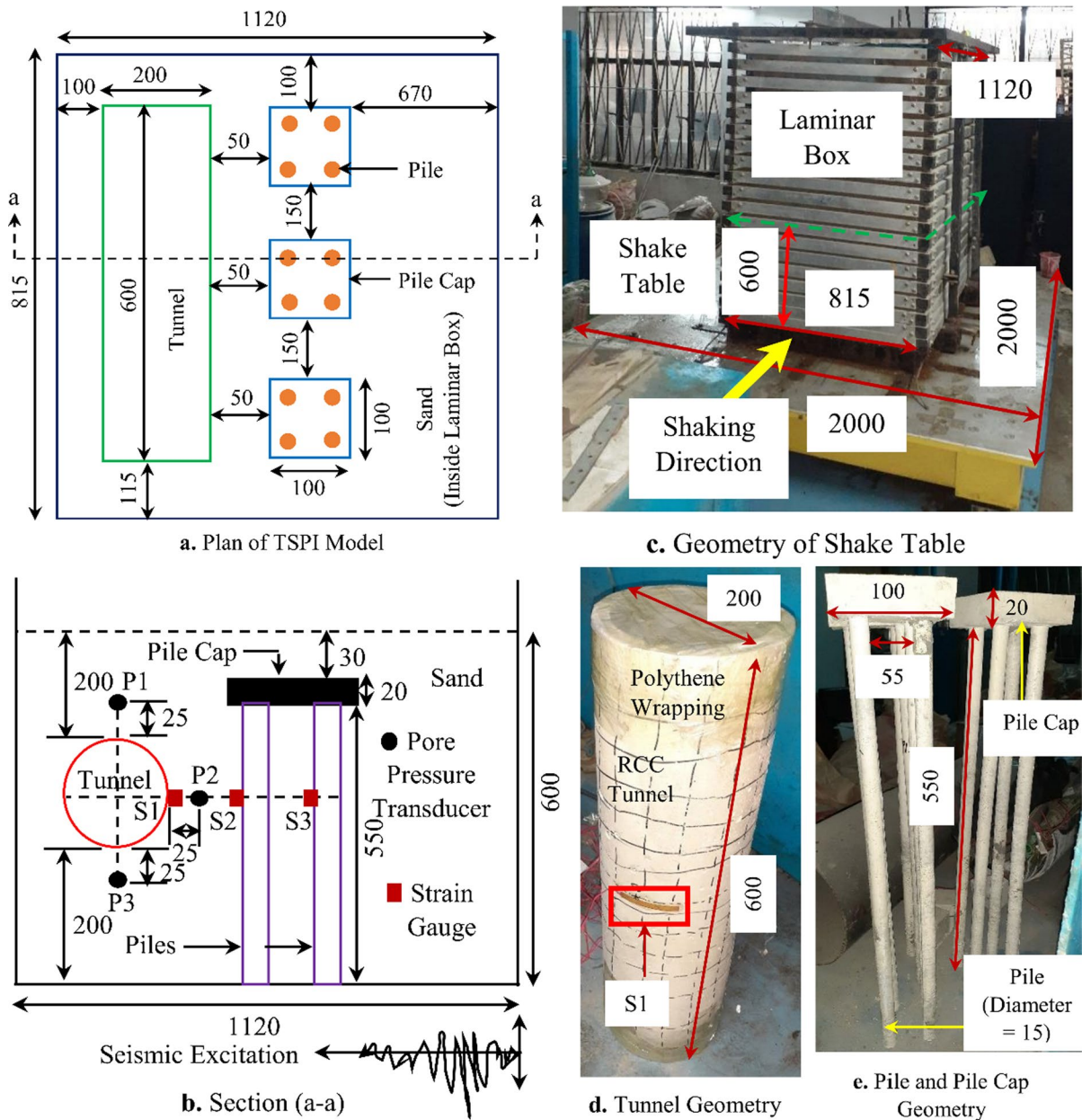


Fig. 1 Geometric properties of shake table and TSPI model parameters (sand, tunnel, pile, and pile cap) with sensors arrangements (Note: i. all dimensions are in millimeters (mm); ii. drawings are not in scale)

ratio of 1:1.25:2.5. For the predicting seismic response of a subway station using a shake table test in the liquefiable ground, 0.7–1.2 mm diameter weir mesh was used as a reinforcement of subway (An et al. 2021). In the present study, a 1 mm diameter weir mesh was used as a reinforcement of the tunnel and pile having a square grid pattern of 25 mm ×

25 mm. The local sand of Bangladesh was used as a fine aggregate. Also, ordinary Portland cement was used as a binder. During the casting of the tunnel and pile, tamping was applied by the 6 mm diameter steel rod to avoid developing honeycomb, cracks, internal voids, etc. A plastic hollow pipe shutter was used during the casting of the 20 mm thick and 200 mm outer

diameter hollow circular tunnel. The tensile test of the Weir mesh was conducted in the laboratory by computer controlled testing machine. During the casting of the tunnel, three cube concrete block was made for the compressive strength test. The size of the cube was maintained to be 50 mm × 50 mm × 50 mm. Tunnel and concrete cubes were cured within a 28-day period. After curing, shuttering was removed from the tunnel body and cube blocks. These blocks were tested in the laboratory by computer-controlled compressive strength testing machine and data was recorded. The fresh concrete tunnel was placed inside the sand medium. The concrete piles and pile caps were prepared to follow the same procedure like as the tunnel. Considering the 4-storied superstructure load and soil condition, the diameter of the pile, length of the pile, thickness, and size of the pile cap were maintained to be 15 mm, 550 mm, 20 mm, and 100 mm × 100 mm, respectively. The mix ratio was used to be 1:1.5:3 for the pile and pile cap. The pile and pile cap was cured within a 28-day period and a compressive strength test was performed for the cube sample of the pile and pile cap. In the pile cap, the weir mesh was provided to maintain two layers. Seven 1 mm diameter weir meshes were spirally confined together to use inside the concrete pile as reinforcement. Each pile cap consists of four piles. Clear spacing between two piles in a single pile cap was maintained to be 55 mm. Details configuration of the pile and pile caps are shown in Fig. 1e. Two faces (start and end) of the tunnel were wrapped by the thin polythene layer and it was tightened by rope. The thin polythene was capable to protect the tunnel from the inside filling of the tunnel by the sand. Details geometry of the tunnel is represented in Fig. 1d. The

material properties of sand were collected from the previous literature (Hossain and Ansary 2018) as shown in Table 4.

$$r_{u,\sigma_v'} = \frac{\sigma_{v0}' - \sigma_v'}{\sigma_{v0}'} = \frac{(\sigma_v - p_0) - (\sigma_v - p_i)}{(\sigma_v - p_0)} = \frac{p_i - p_0}{\sigma_v - p_0} = \frac{\Delta p}{\sigma_{v0}'} \quad (1)$$

$$M = \frac{EI}{y} \varepsilon \quad (2)$$

where, σ_{v0}' = initial effective vertical stress prior to the seismic excitation. σ_v' = current vertical effective stress during the dynamic calculation. p_0 = initial pore pressure. p_i = pore pressure during dynamic calculation. σ_v = total stress. $r_{u,\sigma_v'}$ = excess pore pressure ratio. Δp = change in pore pressure. M = tunnel or pile moment. E = modulus of elasticity. I = moment of inertia with respect to the centroidal axis of the tunnel or pile. y = distance from the center to the top surface of the tunnel or pile. ε = strain.

2.2 Preparation Procedure of the TSPI Model

Sand bed preparation was the first step of the setup of the TSPI model. Three layers were maintained for this bed preparation, and each layer was 200 mm thick. Each layer's relative density of sand was controlled by the Pluviator technique (Hossain and Ansary 2018). A plastic cylindrical box was attached to the cone to form the Pluviator. The height and inner diameter of the plastic cylinder were found to be 450 and 75 mm. The inner diameter of the steel cone was maintained to be 450 mm. The cone was connected to the crane by rope. To control various relative densities of sand, falling height is essential. Therefore, the falling

Table 4 Material properties of weir mesh, tunnel, pile, pile cap, and sand

Materials	Item	Values	Unit	Remarks
Weir Mesh	Tensile stress	568	MPa	Laboratory Test
	Yield stress	437	MPa	
	Elongation	2.6	mm	
Tunnel	28 days average crushing strength	38	MPa	
Pile/Pile Cap	28 days average crushing strength	30	MPa	
Sand	Fineness modulus (FM)	1.01	–	Hossain and Ansary (2018)
	Specific gravity	2.68	–	
	Maximum dry density	16.32	kN/m ³	
	Minimum dry density	12.30	kN/m ³	
	Average diameter of sand, D ₅₀	0.22	mm	

Fig. 2 Recorded accelerations and corresponding frequencies of the Kobe and Loma Prieta seismic excitations

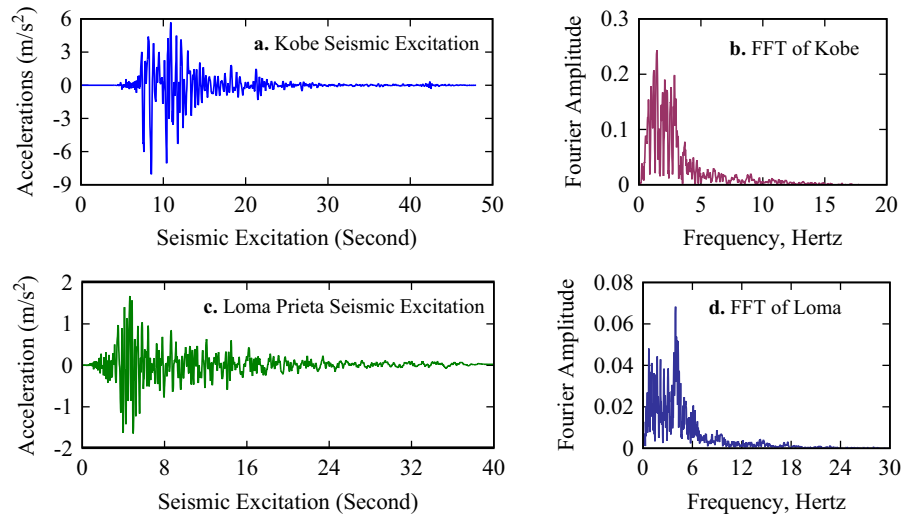
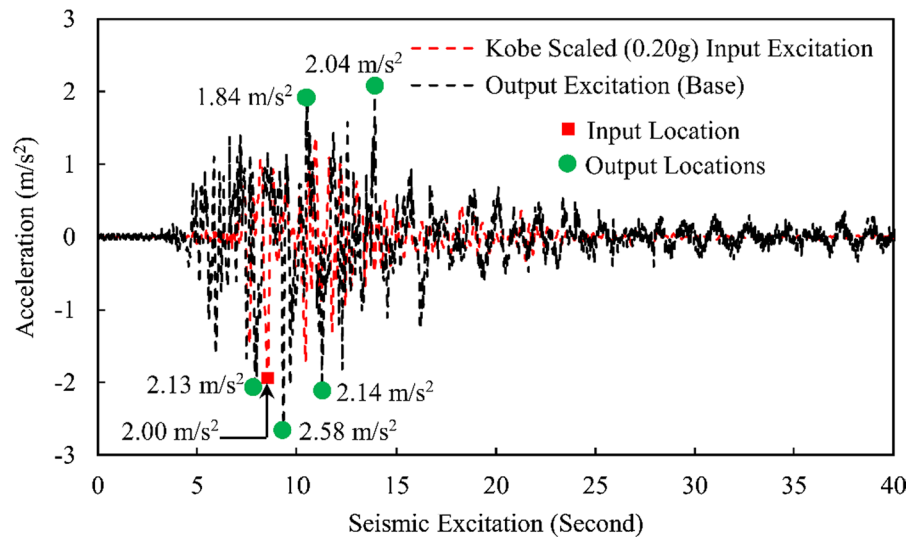


Fig. 3 Calibration of the shake table for the 41% relative density with peak ground acceleration of the Kobe earthquake of 0.20g

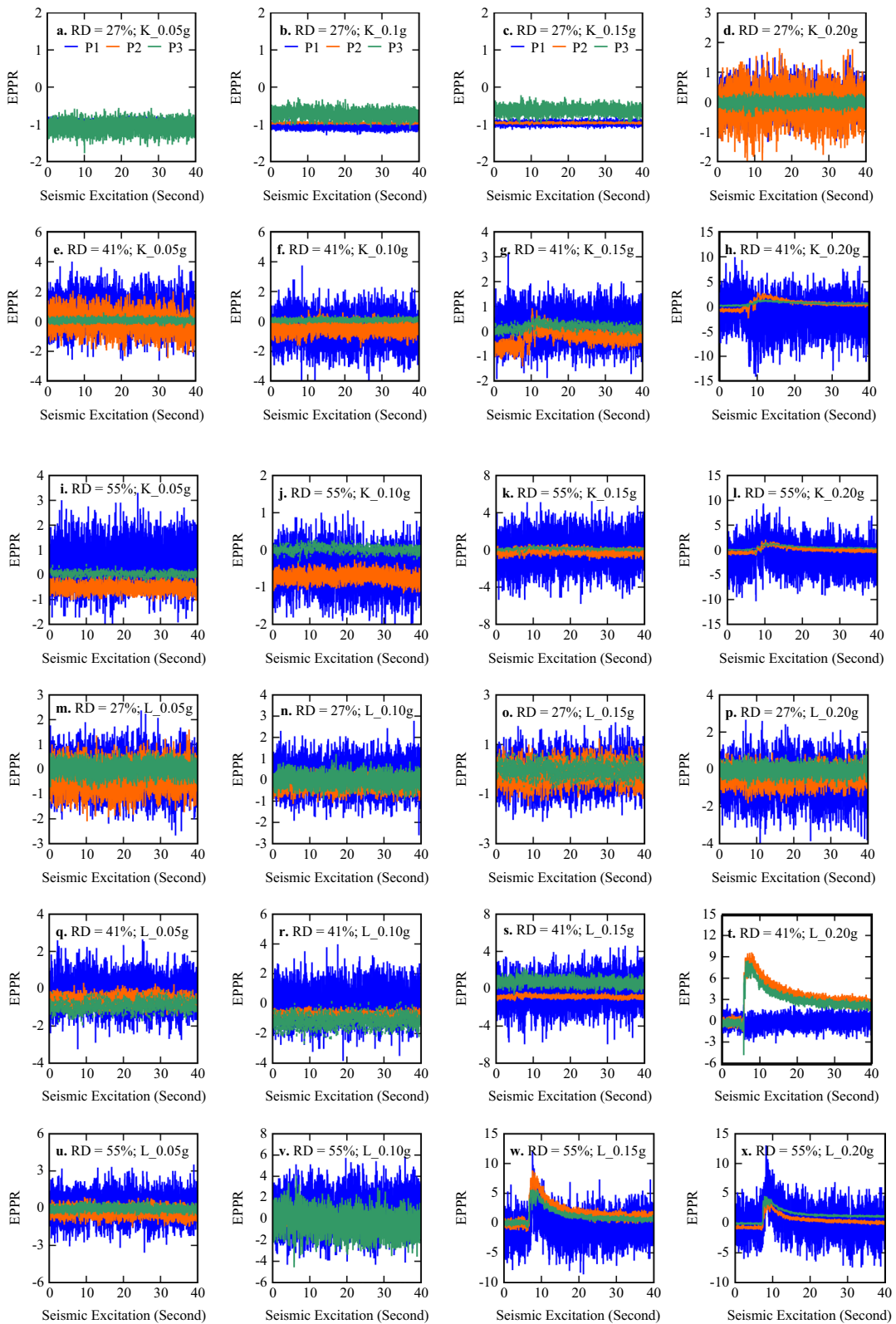


height of 27, 41, and 55% relative densities of sand was maintained to be 100, 200, and 400 mm, respectively according to the previously published work (Hossain and Ansary 2018). Piles with caps were placed inside the laminar box from the beginning and the tunnel stayed in the box after the first 200 mm filled-up of the laminar box by sand. The same relative density was maintained for three layers. To get the liquefaction effect, each layer was fully saturated by mixing water. Fully saturation was ensured by the laboratory test in each stage of sand bed preparation. The tunnel was placed inside the laminar box by helping the crane with the rope. After full saturation of

the whole model, seismic shaking was applied along the transverse direction of the tunnel at the base of the laminar box.

2.3 Input Seismic Excitations

Two types of seismic excitations were applied on the shake table along the center line in only one direction. The centreline of the shake table and the laminar box are maintained to be the same to avoid eccentricity. Kobe and Loma Prieta earthquake records were used in this experimental study after scaling by several factors in terms of gravitational acceleration (*g*). Four



◀**Fig. 4** Variations of the EPPR for different relative densities and peak ground accelerations

peak ground accelerations were used for both earthquakes. These accelerations were 0.05, 0.10, 0.15, and 0.20 g. These accelerations were applicable for the relative densities of 27%, 41%, and 55%. So, a total 24 number of tests were conducted for predicting the interaction response of the TSPI model. Recorded Kobe and Loma Prieta accelerations are shown in Fig. 2a and c. Estimated Fourier amplitudes for both earthquakes are represented in Fig. 2b and d. These recorded excitations were scaled during application at the base of the laminar box on the shake table.

2.4 Calibration of the Shake Table

Calibration of the shake table is necessary to obtain accurate results, so this table was calibrated based on the input and output accelerations responses. Output acceleration response was taken from the base accelerometer. Output acceleration was shown a higher fluctuation rate than input acceleration which informs proper calibration. Calibration was performed for each record of the seismic excitation. One of the calibration records is shown in Fig. 3 for the relative density of 41% and peak ground acceleration of 0.20 g. In this case, output acceleration exceeded four locations from the peak input acceleration, and the maximum value of output acceleration was found to be 2.58 m/s². Maximum output acceleration was 29% higher than input acceleration. Other ordinates of the output accelerations fluctuated at a higher rate than the input acceleration in Fig. 3.

2.5 Development of Excess Pore Pressure Ratio (EPPR) Surrounding Tunnel Body

The concrete TSPI response using a shake table is a novel technique. So, no existing literature is matched to the present research. Recently, a shake table test was performed for the steel utility tunnel only on the liquefiable ground using a shake table (Yue et al. 2021). They used Wenchuan and EI Centro records considering different peak ground accelerations (PGA). Liquefaction existed (EPPR exceeds unit value) at several locations surrounding the tunnel body based on that study. However, in the present research, pore pressure transducers (P1, P2,

and P3) were placed in three locations from 25 mm away from the tunnel body in Fig. 1b for the estimation of the excess pore pressure ratio (EPPR). EPPR was calculated for 24 tests. Variations of EPPR are shown in Fig. 4 for relative densities of 27%, 41%, and 55% with the different peak ground accelerations (0.05, 0.10, 0.15, and 0.20 g) of both earthquakes (Kobe and Loma Prieta). Liquefaction exists when a change in pore pressure inside the soil body is equal to or greater than the initial effective vertical stress. In this situation, soil catastrophically loses its shear strength due to the eruption of the sand boils in undrained conditions during seismic excitation. Negative EPPR was developed due to the dilatancy of soil for many cases of experimental tests. The fluctuation rate of the EPPR at the location of 25 mm above the tunnel crown (P1) in Fig. 4 is higher than almost all cases except for the relative density of 41% with a PGA of 0.20 g. The main reason for higher EPPR at P1 is the close position surrounding the tunnel body and near the surface of the TSPI model. The seismic impact is higher at the upper part of the sand and surrounding area of the tunnel body. Another reason for the higher EPPR is the scattering effect of transverse seismic excitation because the larger volume of the tunnel can be capable to divert lateral seismic force to the vertical due to the existence of the undrained situation within a short period. The stiffness of the deeper soil is larger than shallower/upper soil because of the higher over-burden pressure in the deeper soil. The stiffness of the soil is inversely proportional to the material as well as radiation damping. Therefore, most of the seismic excitations are passed through the deeper/lower sand layer. When it reached close to the tunnel then the existence of the scattering effect impacts the build-up EPPR. EPPR is build-up suddenly in any location because of the existence of undrained conditions during seismic excitation. Displacement is suddenly higher due to the undrained condition. For this reason, stress decreases and EPPR increases because of inverse proportionality. The sudden increase of the EPPR at locations of P2 and P3 informs the existence of undrained conditions for the 41% relative density having a PGA of 0.20 g. Most of the cases, liquefaction does not exist at the P3 location in Fig. 4 because of the transfer mechanism of strain energy to the adjacent sand particle prior eruption of sand boils due to the nonlinearity and anisotropic properties. EPPR ratio varies from

Table 5 Variations of excess pore pressure ratio for different seismic excitations and relative densities

Test No	RD (%)	Excitation Type	“g” Factors	Excess Pore Pressure Ratio (EPPR)								
				P1			P2			P3		
				Max	Min	RMS	Max	Min	RMS	Max	Min	RMS
1	27	Kobe	0.05	-0.73	-1.13	0.93	-0.89	-1.03	0.95	-0.56	-1.77	1.09
2	0.10		-0.85	-1.29	1.07	-0.89	-1.03	0.96	-0.28	-1.13	0.74	
3	0.15		-0.78	-1.15	0.97	-0.90	-1.03	0.96	-0.22	-0.98	0.63	
4	0.20		1.58	-1.71	0.44	1.81	-2.45	0.55	0.35	-0.50	0.12	
5	41	0.05	4.01	-2.63	1.12	2.04	-2.48	0.70	0.58	-0.48	0.13	
6		0.10	3.74	-4.37	1.13	0.83	-1.79	0.63	0.44	-0.26	0.12	
7		0.15	3.12	-1.92	0.63	0.92	-1.42	0.39	0.67	-0.33	0.22	
8		0.20	9.94	-14.11	3.60	2.79	-2.42	0.95	1.34	-0.23	0.62	
9	55	0.05	3.30	-1.97	0.90	0.16	-1.09	0.56	0.44	-0.32	0.10	
10		0.10	1.06	-2.13	0.74	-0.25	-1.20	0.74	0.32	-0.35	0.09	
11		0.15	5.24	-5.80	1.70	0.78	-1.15	0.34	0.73	-0.63	0.17	
12		0.20	9.35	-10.33	3.02	2.08	-1.17	0.52	1.64	-0.84	0.58	
13	27	Loma Prieta	0.05	2.37	-2.67	0.71	1.60	-2.10	0.61	0.84	-0.83	0.25
14	0.10		2.77	-2.60	0.67	0.59	-1.14	0.36	1.22	-0.96	0.28	
15	0.15		1.89	-2.11	0.60	1.24	-1.49	0.42	0.80	-0.98	0.27	
16	0.20		2.66	-4.35	1.16	0.90	-1.85	0.59	1.11	-1.05	0.27	
17	41	0.05	2.64	-3.25	0.80	0.32	-1.52	0.64	-0.03	-2.00	0.95	
18		0.10	3.97	-3.84	1.01	-0.05	-1.20	0.68	0.24	-2.87	1.22	
19		0.15	4.61	-5.95	1.52	-0.31	-1.32	0.83	2.26	-0.64	0.80	
20		0.20	2.44	-3.18	0.81	9.69	-1.43	4.04	8.60	-4.70	3.47	
21	55	0.05	3.52	-3.58	0.97	0.90	-1.55	0.48	0.77	-0.76	0.20	
22		0.10	5.82	-4.31	1.65	0.19	-1.36	0.55	4.06	-4.56	1.11	
23		0.15	12.05	-8.61	2.46	8.83	-1.44	2.43	5.67	-0.86	1.69	
24		0.20	13.03	-7.45	2.57	3.78	-1.25	0.95	4.55	-0.44	1.59	

The bold form represents the maximum values (RMS and SRSS)

10 to 15 for some cases in Fig. 4 because of different Poisson's ratios in three orthogonal directions due to the anisotropic behaviors of sand. This variation informs higher hysteretic degradation of the sand boil as well as the very bad condition of sand. In all cases, liquefaction exists at the P2 location (interaction zone) in some certain/full excitation period because of the simultaneous impact of the tunnel and pile. In this location, it is very difficult to evaluate the actual response of sand because of the existence of various reflected, transmitted, and scattered waves from the tunnel, pile, and sand. However, simultaneous impacts of various waves at the P2 location may reduce the EPPR from the P1 and sometimes P3. The root mean square (RMS) value of the EPPR is necessary to predict the average impact of various forces

on a point within a specific period due to seismic excitation. So, maximum (Max.), minimum (Min.), and RMS values of various peak ground accelerations containing seismic excitations are shown in Table 5. These values are recorded for various relative densities. Maximum RMS responses of various locations surrounding the tunnel body may be considered as a standard for further large-scale study or practical construction. Maximum RMS responses of the P1, P2, and P3 locations are calculated to be 3.60, 4.04, and 3.47, respectively. RMS response shows a maximum value at the interaction zone among them because of the simultaneous impact of the tunnel and piles.

2.6 Variations of Tunnel and Pile Moments in Liquefiable Sand

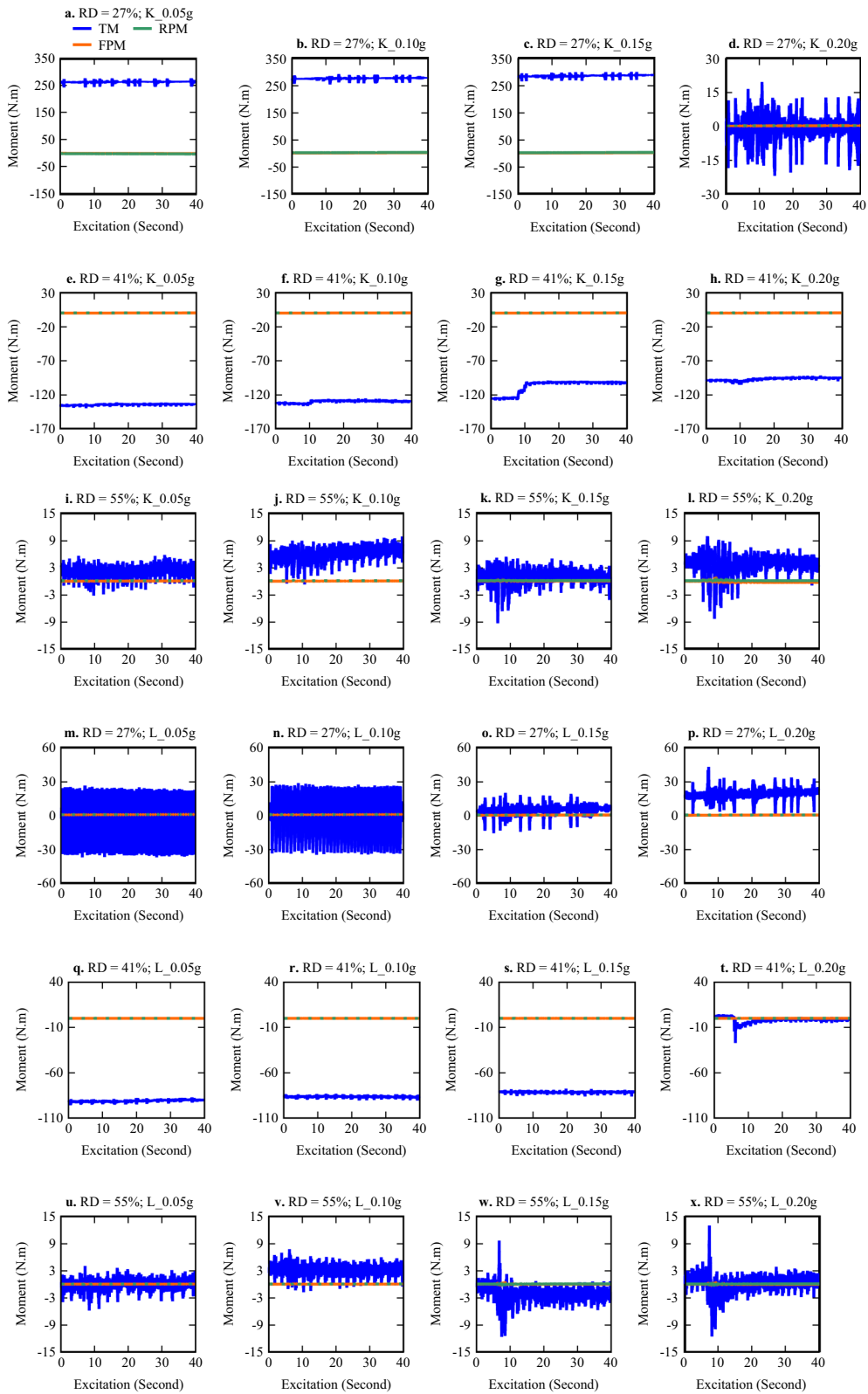
The interactive tunnel and pile moments are scarce in the literature. Although individual tunnel (Yue et al. 2021; Wang et al. 2022) and pile (Sahare et al. 2022) moment variations are available in the recent literature. In this research, the interactive tunnel and pile moments are calculated from the strain gauge readings of S1 (right face of the tunnel), S2 (front pile), and S3 (rear pile) locations within the interaction zone. The representation of these locations is shown in Fig. 1b. The moment is calculated by using Eq. (2). The strain was taken during the test by using strain gauges. Variations of the moments are depicted in Fig. 5 for the peak ground accelerations of 0.05, 0.10, 0.15, and 0.20 g with relative densities of 27, 41, and 55%. The duration of these peak ground accelerations is estimated from the recorded Kobe and Loma Prieta earthquakes. In all cases, the tunnel moment (TM) is larger than the front pile moment (FPM) and rear pile moment (RPM). The main reason for the larger moment is the heavier volume and stiffness of the tunnel compared to the adjacent piles. The moment is proportional to the flexural rigidity. This rigidity is the function of the volume, so higher volume increases tunnel moment due to the seismic excitation. This concept is valid for comparison with the lower volume pile. Most of the cases, front and rear pile moments are closely varied from each other because of the same material properties and size. The surrounding zone of the tunnel is liquefied during seismic excitation based on the shake table test. So, liquefiable sand impacts the tunnel body along with the seismic excitation. This phenomenon is responsible for the increment of the tunnel moment. The fluctuation rate of the average tunnel moment varies from 10 to 15 N–m based on the experimental results in Fig. 5. The difference between the tunnel and pile moments is found to be approximately 100 N–m in Fig. 5 for the relative densities (27% and 41%) and peak ground accelerations (0.05, 0.10, and 0.15 g). The main reason for the higher variation of the moment may be the occurrence of the resonance of the tunnel during excitation because of the similar variations of predominant exciting and tunnel natural frequencies. Average variations of moment between tunnel and piles are found to be 10 N–m in Fig. 5 for the 55% relative density with the

peak ground accelerations of 0.05, 0.10, 0.15, and 0.20 g. Piles are smaller elements compared to the tunnel, so the impact of piles on the tunnel body is very less based on the shake table test results. The fluctuation rate of the tunnel moment is varied within the excitation period because of the variations of the predominant frequencies. The maximum tunnel moment is 130 N–m at 41% relative density with peak ground accelerations of 0.05, 0.10, and 0.15 g for the recorded Kobe excitation in Fig. 5. The square root sum of squares (SRSS) or resultant moment is necessary for the design of a tunnel because of a series of non-uniform forces acting on the tunnel body within a certain period. In addition, it is required to learn about the root mean square (RMS) value along with the maximum (Max.), minimum (Min.), and SRSS values. Therefore, maximum, minimum, RMS, and SRSS variations of the tunnel, front pile, and rear pile moments are represented in Table 6. Maximum SRSS values for the tunnel, front pile, and rear pile are calculated to be 18,662, 26, and 19 N–m, respectively. 27% relative density with peak ground acceleration of 0.15 g of recorded Kobe earthquake shows the maximum SRSS and RMS values of the tunnel in Table 6. Similarly, 27% relative density with peak ground acceleration of 0.10 g of recorded Loma Prieta earthquake represents the maximum SRSS and RMS values of the front and rear piles.

3 Numerical Study

3.1 Methodology of Numerical TSPI Model

The full-scale tunnel-sand-pile interaction (TSPI) model is performed numerically. Finite element-based software, Plaxis conducts this three-dimensional analysis. Three stages are followed for the preparation of the geometry. The volume of sand is created in the first stage. In this stage, no load is applied to the model. The tunnel is inserted into the sand by deactivating the sand volume inside the tunnel. Dry condition is selected inside the circular tunnel. In the third stage of construction, piles along with caps are placed inside the sand. A negative interface is chosen for the tunnel. Positive and negative interfaces are considered for the pile caps. The interface is provided to get the interaction effect among the tunnel, sand, and piles along with caps. Sand and



◀**Fig. 5** Variations of the tunnel and pile moments for different relative densities and peak ground accelerations

pile are considered to be 10-nodded tetrahedral (volume) and 2-nodded line elements. For the numerical integration, 4-point and 3-point Gauss integrations are performed for the volume and line elements. Tunnel and pile caps are considered to be the 6-nodded triangular element, which is solved by the 3-point Gauss integration technique. The average dimension of the element is taken to be 100 mm for performing meshing. Seismic excitation is applied at the base of the model along the transverse direction of the tunnel. The bottom boundary of the model is considered to be fixed because of the fixed aluminum plate attached to the bottom of the shake table. All sides of the TSPI model are taken to be hinges because the whole model was prepared inside the laminar box on the shake table. The top of the model is assumed to be free. The geometric configuration with the boundary condition of the numerical TSPI model is shown in Fig. 6a. Volume and plate elements are represented in Fig. 6b and c, respectively. Before run analysis, pore pressure and strain locations are marked inside the numerical TSPI model like-as an experimental setup. Four types of seismic excitations are applied for the numerical analysis to compare the generating results with the experimental results. These excitations are (a) 41% relative density with peak ground acceleration of recorded Kobe earthquake of 0.20 g, (b) 41% relative density with peak ground acceleration of recorded Loma Prieta earthquake of 0.20 g, (c) 27% relative density with peak ground acceleration of recorded Kobe earthquake of 0.15 g, and (d) 27% relative density with peak ground acceleration of recorded Loma Prieta earthquake of 0.10 g.

3.2 Constitutive Models

3.2.1 UBC3D-PLM (Liquefaction Model) for Sand

UBC3D-PLM means the University of British Columbia Plaxis liquefaction model considering three-dimensional effect. The UBC3D-PLM model is formulated from the original two-dimensional model of the UBCSAND. The original UBCSAND (Puebla et al. 1997; Beaty and Byrne, 1998) was formulated in the classical plasticity theory with a hyperbolic

strain hardening role, based on the original Duncan-Chang model. The main differences between the UBC3D-PLM and UBCSAND models are (a) adding the mechanism of the 3D formulation, and (b) using a modified non-associated plastic potential function based on Drucker-Prager's criterion in lieu of the hyperbolic strain hardening rule based on the original Duncan-Chang model. Drucker-Prager's criterion was used for the primary yield surface to maintain the assumption of stress–strain coaxiality in the deviatoric plane for a stress path beginning from the isotropic line (Tsegaye 2010). However, identifications of the input parameters of the Plaxis liquefaction model are listed herein (Plaxis 2020).

- (a) Stress-dependent stiffness according to a power law ($k_B^{*e}, k_G^{*e}, me, ne, np$)
- (b) Plastic straining due to primary deviatoric loading (k_G^{*p})
- (c) Densification due to the number of cycles during secondary loading ($f_{dens.}$)
- (d) Post-liquefaction stiffness degradation ($f_{Epost.}$)
- (e) Failure according to the Mohr–Coulomb failure criterion ($\varphi_{cv}, \varphi_p, and c$)

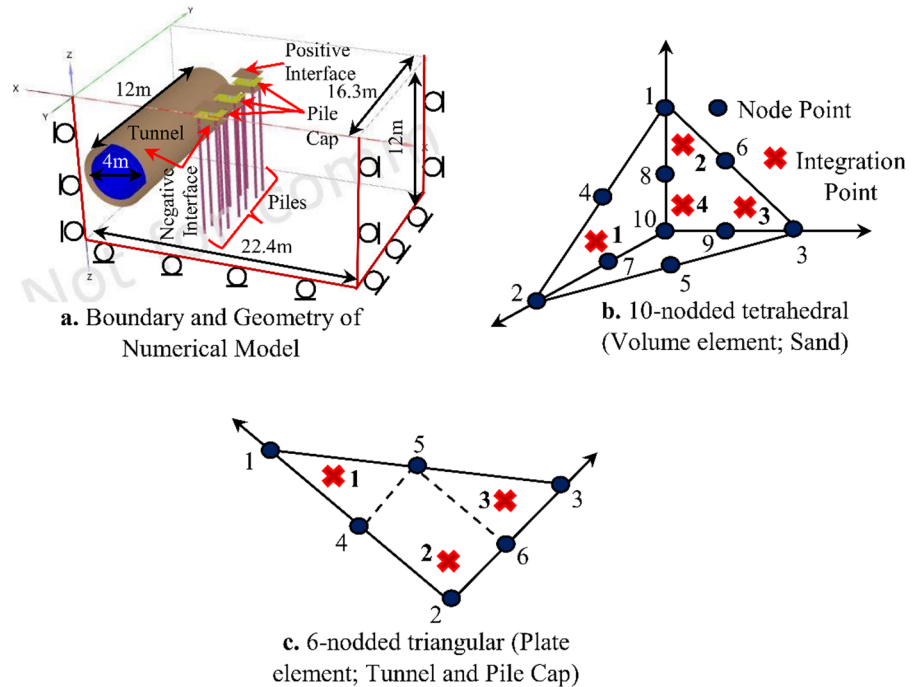
The UBC3D-PLM model incorporates a non-linear, isotropic law for elastic behavior. This model is defined in terms of the elastic bulk modulus (K) and the elastic shear modulus (G). The elastic bulk and shear moduli are defined by Eqs. (3) and (4). The ratio between the effective (p') and reference ($p_{ref.}$) pressures are the function of the bulk and shear moduli. The implicit Poisson's ratio is calculated by using Eqs. (3) and (4). The UBC3D-PLM model introduces two yield surfaces to get a smooth transition into the liquefied state of the soil to enable the distinction between primary and secondary loadings in Fig. 7. This model incorporates a densification law through a secondary yield surface with a kinematic hardening rule that improves the precision of the evaluation of the excess pore pressure. This surface generates lower plastic deformations compared to the primary yield surface. Beaty and Byrne (2011) proposed equations of the elastic shear modulus (k_G^{*e}), elastic bulk modulus (k_B^{*e}), and plastic shear modulus (k_G^{*p}) for the initial generic calibration of the UBCSAND. Makra (2013) revised the proposed equations and highlighted the differences between the original UBCSAND 2D formulation and the UBC3D-PLM

Table 6 Variations of tunnel and pile moments for different seismic excitations and relative densities

Test No	RD (%)	Excitation Type	“g” Factors						Moments (N–m)					
			Tunnel (S1)			Front Pile (S2)			Rear Pile (S3)					
			Max	Min	RMS	SRSS	Max	Min	RMS	SRSS	Max	Min	RMS	SRSS
1	27	Kobe	277.90	242.21	263.56	17,192	0.24	0.21	0.23	15	0.15	0.07	0.13	9
2			292.56	254.67	276.57	18,041	0.26	0.22	0.24	16	0.16	0.05	0.13	9
3			299.73	266.41	286.09	18,662	0.27	0.24	0.25	17	0.16	0.00	0.13	9
4			19.60	-21.92	5.16	337	0.02	-0.02	0.01	0.43	0.04	-0.18	0.02	1.32
5	41		-131.18	-139.63	134.49	8774	0.02	-0.02	0.00	0.24	0.04	0.00	0.01	0.72
6			-125.31	-136.67	129.96	8478	0.03	-0.02	0.01	0.38	0.05	-0.01	0.02	1.02
7			-99.42	-128.64	107.59	7018	0.06	-0.04	0.01	0.86	0.09	-0.01	0.03	1.93
8			-91.90	-105.54	97.06	6332	0.16	-0.26	0.05	3.12	0.23	-0.07	0.07	4.30
9	55		5.79	-3.17	2.45	160	0.14	-0.06	0.04	2.74	0.13	-0.01	0.01	0.62
10			9.84	-0.68	6.26	409	0.18	-0.08	0.05	3.23	0.18	-0.01	0.02	1.03
11			5.45	-9.25	1.77	116	0.41	-0.11	0.07	4.43	0.23	-0.03	0.03	2.07
12			10.01	-8.28	4.18	273	0.88	-0.53	0.32	21	0.47	-0.10	0.09	5.70
13	27	Loma Prieta	26.65	-37.08	13.40	874	0.42	0.34	0.39	25	0.32	0.22	0.28	19
14			28.72	-34.67	13.42	876	0.43	0.34	0.39	26	0.32	0.19	0.29	19
15			20.19	-15.46	6.55	428	0.02	-0.01	0.01	0.49	0.04	-0.10	0.01	0.54
16			43.12	-0.42	19.74	1288	0.06	0.00	0.03	1.68	0.06	-0.14	0.01	0.77
17	41		-87.13	-95.79	89.95	5868	0.08	0.01	0.05	3.23	0.19	-0.03	0.06	3.74
18			-83.12	-90.68	85.84	5600	0.09	0.00	0.05	3.36	0.21	-0.03	0.07	4.29
19			-77.54	-86.16	80.23	5234	0.13	-0.05	0.06	3.75	0.25	-0.05	0.08	5.18
20			4.65	-26.95	3.20	209	0.24	-0.34	0.08	5.10	0.38	-0.11	0.09	6.14
21	55		4.05	-5.79	1.08	70.22	0.17	-0.07	0.02	1.17	0.17	-0.15	0.03	1.77
22			7.77	-1.73	3.28	215	0.23	-0.10	0.03	2.02	0.19	-0.18	0.03	2.26
23			9.67	-11.61	2.71	177	0.51	-0.36	0.08	5.11	0.22	-0.34	0.06	3.80
24			13.01	-11.53	1.77	116	0.45	-0.36	0.09	5.78	0.24	-0.37	0.06	4.18

The bold form represents the maximum values (RMS and SRSS)

Fig. 6 Geometry and element formulations of the TSPI model for the numerical analysis



model, as implemented in Plaxis. The proposed equations for the generic initial calibration are the function of the corrected standard penetration number $((N_1)_{60})$. The corrected standard penetration number (SPT) is the function of the relative density. So, equations of the elastic shear modulus factor, elastic bulk modulus factor, plastic shear modulus factor, and corrected field SPT are represented by Eqs. (5), (6), (7), and (8), respectively. The present study uses three relative densities of sand. So, stiffness factors are calculated directly by using these equations because of the function of the relative density. The peak friction angle (φ_p) is the function of the constant volume friction angle. The constant volume friction angle (φ_{cv}) is taken to be the friction angle (φ) of sand because of avoiding complexity. The peak friction angle is expressed in Eq. (9). Hansen (1970) provided a correlation for the calculation of the friction angle of sand as expressed in Eq. (10). In this research, atmospheric pressure is taken to be the reference pressure to conduct the liquefaction analysis. The parameters of the UBC3D-PLM model are shown in Table 7.

$$K = k_B^{*e} p_{ref.} \left(\frac{p'}{p_{ref.}} \right)^{me} \tag{3}$$

$$G = k_B^{*e} p_{ref.} \left(\frac{p'}{p_{ref.}} \right)^{ne} \tag{4}$$

$$k_G^{*e} = 21.7 \times 20 \times (N_1)_{60}^{0.333} \tag{5}$$

$$k_B^{*e} = 0.7 \times k_G^{*e} \tag{6}$$

$$k_G^{*p} = k_G^{*e} \times (N_1)_{60}^2 \times 0.003 + 100 \tag{7}$$

$$(N_1)_{60} = \frac{RD^2}{15^2} \tag{8}$$

$$\varphi_p = \varphi_{cv} + \frac{(N_1)_{60}}{10} + \max. \left(0; \frac{\{(N_1)_{60} - 15\}}{5} \right) \tag{9}$$

$$\varphi(deg) = (26^0 + 10D_r + 1.6\log D_{50}) \tag{10}$$

3.2.2 Elasto-Plastic Concrete Model for Tunnel, Pile, and Pile Cap

Materials of the tunnel, pile, and pile cap are considered to be concrete. Elasto-plastic concrete

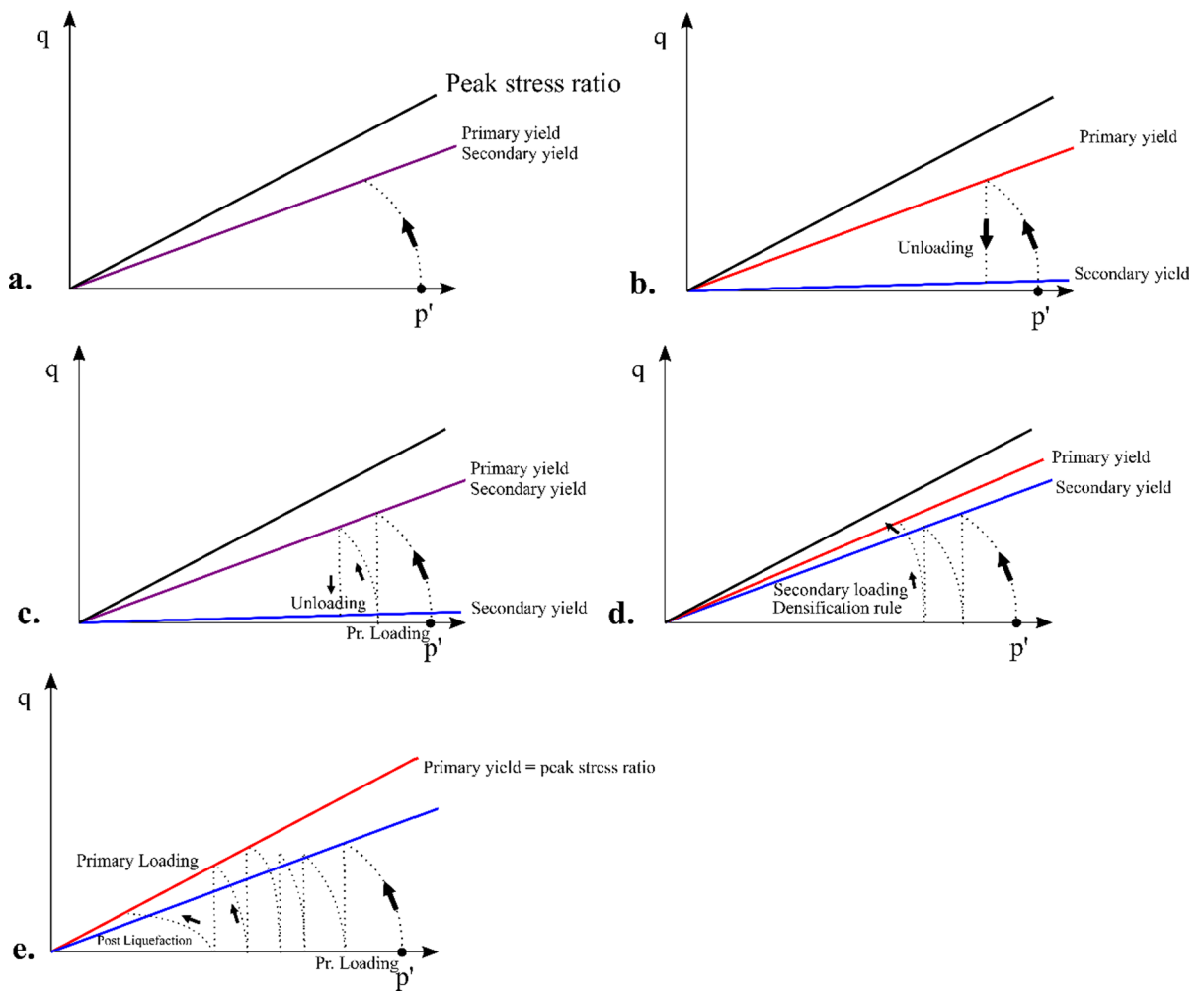
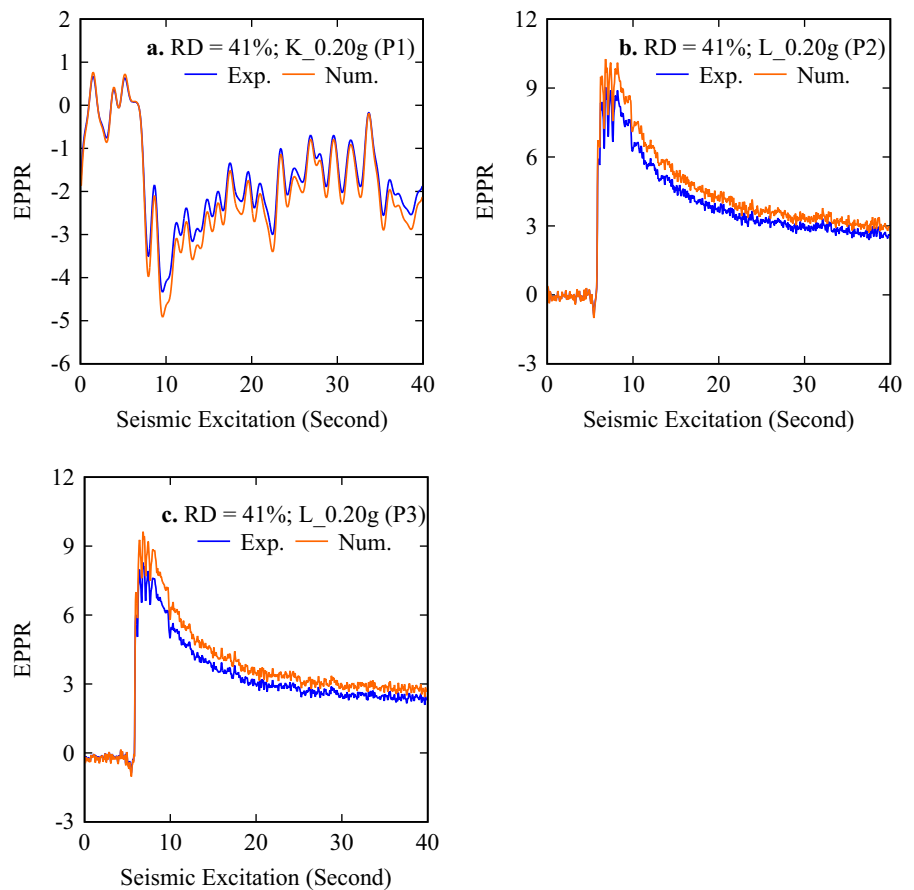


Fig. 7 Representation of yield surfaces of various loadings (after, Plaxis 2020)

Table 7 Parameters of the local sand for the UBC3D-PLM model

Item Description	Relative Density, D_r (%)			Remarks
	27	41	55	
Angle of internal friction, φ (deg) or φ_{cv}	28.3	29.7	31.1	Equation (10)
Dilatancy angle, ψ (deg)	0	0	1.1	Bolton (1986)
Corrected SPT value, $(N_1)_{60}$	3.24	7.47	13.44	Equation (8)
Elastic shear stiffness, k_G^{*e}	642	848	1031	Equation (5)
Elastic bulk stiffness, k_B^{*e}	449.4	593.6	721.7	Equation (6)
Plastic shear stiffness, k_G^{*p}	120.2	242	658.7	Equation (7)
Stress dependency factors; m_e, n_e	0.5	Beatty and Byrne (2011)		
Stress dependency factor, n_p	0.4			
Failure ratio, R_f	0.9			
Stiffness factors; f_{dens}, f_{Epost}	1.0	Petalas and Galavi (2012)		
Peak friction angle, φ_p (deg)	28.62	30.45	32.44	Equation (9)

Fig. 8 Numerical and experimental variations of the EPPR in various locations under seismic excitations



model is taken for the numerical analysis. The concrete model was originally developed to model the behavior of shotcrete, but it is also useful for soil reinforcement, soil improvements, and concrete structures (Plaxis 2020). This elasto-plastic model is used for simulating the time-dependent strength and stiffness of the concrete, strain hardening–softening in compression and tension as well as creep and shrinkage (Schadlich and Schweiger 2014). When subjected to deviatoric loading, concrete shows different behaviors: (a) in compression, the strength increases non-linearly up to a peak value and then softens to a residual one; (b) in tension, it’s considered linear elastic until reaching the tensile strength and then softens to the residual value (Plaxis 2020). In addition, this model employs a Mohr–Coulomb yield surface for deviatoric loading, combined with a Rankine yield surface in the tensile regime. This model can be derived from standard uniaxial tension and compression tests. The composite yield

surface expresses the Mohr–Coulomb surface for deviatoric loading and the Rankine surface in the tensile regime with isotropic compression softening. In tension, the tensile failure strain is derived from the cured concrete’s tensile fracture energy and tensile strength, regardless of the current concrete age. In shotcrete linings, tensile strength is essential for tunnel stability (Plaxis 2020). Incremental stiffness of structures exhibits non-linear plastic behaviors.

3.3 Numerical Analysis Procedure

Numerical analysis is conducted by the stiffness formulations of the various elements. During the seismic excitation, this analysis is performed by Newmark’s method. The implicit time integration scheme of Newmark is a frequently used method. According to the average acceleration method, Newmark’s alpha and beta coefficients are considered to be 0.25 and

Fig. 9 Numerical and experimental variations of the tunnel and pile moments in various locations under seismic excitations

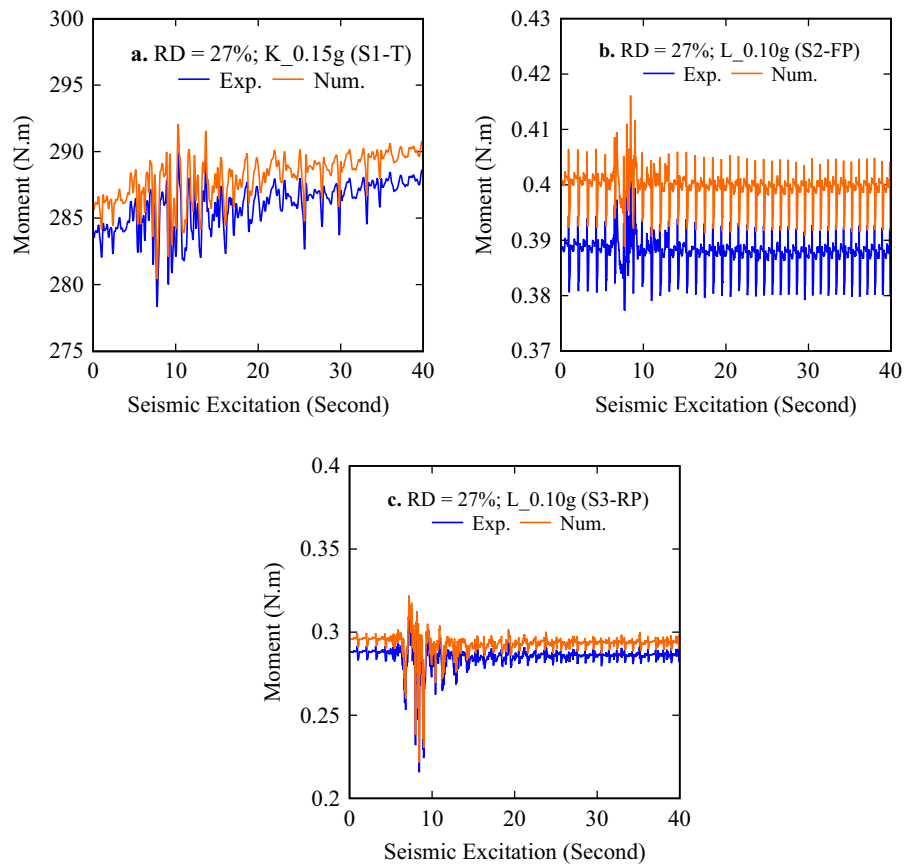
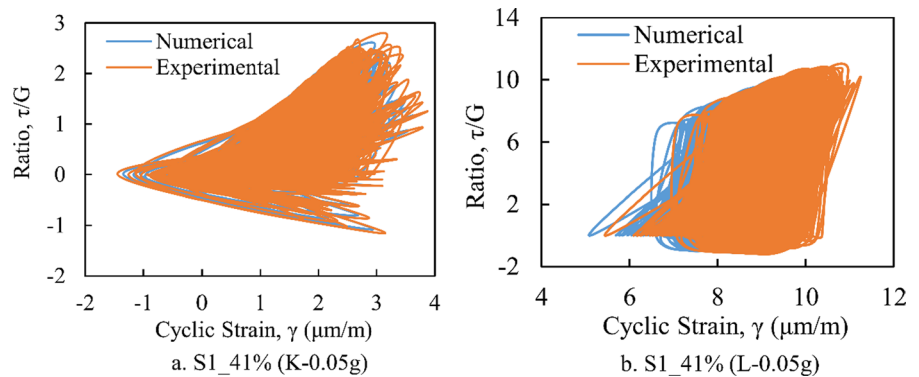


Fig. 10 Numerical and experimental variations of cyclic strain of the tunnel in interaction zone under seismic excitations



0.5, respectively (Plaxis 2020). The critical time step is advantageous for the implicit calculation, and the critical time step depends on the finite element mesh's maximum frequency and fineness. The critical time step is the ratio between the minimum length between two nodes of an element and the shear wave velocity of this element (Plaxis 2020). Dynamic integration coefficients are the functions of the alpha, beta, and

critical time steps. During analysis, the sand medium is considered to be homogeneous, isotropic, and infinite. Displacement is set to zero at the starting time of the analysis. The number of loading, unloading, and reloading steps is automatically selected by the software until convergence is achieved including 5% tolerance because of reducing time and complexity.

3.4 Comparison of Numerical and Experimental Results

Experimental results are compared with the numerical study to obtain close variations of both results. Numerical analysis is performed for the large-scale (prototype) of the TSPI model. Variations of the excess pore pressure ratio (EPPR) with the seismic excitation for the numerical and experimental studies are shown in Fig. 8. These variations are represented for the P1, P2, and P3 locations. EPPR of the P1, P2, and P3 locations of both studies are estimated for the 41% relative density with peak ground acceleration of recorded Kobe and Loma Prieta earthquakes of 0.20 g in Fig. 8. The difference in EPPR between the numerical and experimental studies in three locations is varied by approximately (5–10) % during the whole duration of the seismic excitation. In addition, variations of EPPR for P2 and P3 locations are very close for both studies because of the larger impact rate of transverse directional excitation at tunnel invert and interaction zone than other locations. Similarly, experimental and numerical variations of the tunnel moment (S1), front pile moment (S2), and rear pile moment (S3) are represented for the peak ground accelerations of the recorded Kobe earthquake of 0.15 g and Loma Prieta earthquake of 0.10 g, respectively for the 27% relative density showing in Fig. 9. A similar difference in results of the tunnel and pile moments like EPPR between experimental and numerical studies is found during the almost whole duration of the seismic excitation. The incremental cyclic strain (γ) of the tunnel in the interaction zone (S1) fluctuates with variations in dynamic time. Plastic cyclic stress depends on the incremental cyclic strain and shear modulus. A hysteretic loop creates with the variations of cyclic stress ratio (τ/G). Variations of cyclic strain versus cyclic stress ratio are shown in Fig. 10a and b for Kobe and Loma Prieta earthquakes with peak ground acceleration of 0.05 g with 41% relative density. The fluctuation rate of the Loma Prieta earthquake is larger than the Kobe earthquake because of the higher predominant frequency of the Loma Prieta earthquake. The difference in results between numerical and experimental studies lies (5–8) % in most of the fluctuated parts for both excitations. The maximum cyclic stress ratios of experimental and numerical studies are found to be 2.8 and 2.6 respectively, for the

scaled Kobe earthquake. In this case, the difference in result is 7.7%. In the case of the scaled Loma Prieta earthquake, the minimum values of the cyclic strain of experimental and numerical studies are found to be 5.4 and 5.1 $\mu\text{m/m}$, respectively. The difference in results is obtained to be 5.9% in this case.

4 Conclusion

This paper studied variations of the tunnel and pile moments in liquefiable sand under seismic excitations. For this purpose, a shake table test was conducted for the evaluation of the TSPI response. Also, the shake table was calibrated, and results were compared with a numerical study using a liquefaction constitutive model of sand. Therefore, the major results are summarized herewith:

- The EPPR exceeds the unit value based on the experimental results in most cases near the tunnel crown and the interaction zone. The existence of liquefaction is confirmed by the unit value exceedance of the EPPR. In most cases, higher EPPR shows near the tunnel crown because of reducing shear strength of sand due to the scattering phenomenon of the seismic wave. Scattered wave increases excess pore water pressure inside the sand particle because of the generation of extra force by the reflected wave from the tunnel body. In the interaction zone, two opposite-directional reflected waves from the tunnel and pile bodies minimize the development of the excess pore pressure inside the sand particle. The same reason is applicable to the tunnel invert. There is no option to minimize reflected seismic waves from the tunnel body near the tunnel crown because of the free surface at the top of the TSPI model. Therefore, a higher value of the EPPR exists near the tunnel crown than in the other two locations.
- The tunnel, front pile, and rear pile moments are calculated from the same aligned strain gauge reading. The interactive tunnel moment is higher than the front and rear pile moments based on the experimental results because of the larger volume and stiffness of the tunnel. On the other hand, the front and rear pile moments are close to each other because of the same geometry and stiffness. In all cases of relative densities and seismic excitations,

pile moments are small because of the eruption of sand boils in the interaction zone due to the several directional reflected waves from the tunnel and pile bodies. For this reason, excess pore water pressure inside the sand particles in the interaction zone moves other locations of the TSPI model. So, the shear strength of sand is improved in the interaction zone. Therefore, lateral deflection and strain of piles show a smaller value which causes lower moments of piles.

- The EPPR, moments, and cyclic strain variations are addressed for the comparison between the experimental and numerical studies. The comparison results are closely varied which may inform to enhance this research in the future. However, it can be said that the present research may be used to add in the design code as a standard.

Funding The authors declare that no funds, grants, or other support were received during the preparation of this manuscript.

Data Availability The datasets generated during and/or analysed during the current study are not publicly available due to some restriction but are available from the corresponding author on reasonable request.

Declarations

Conflict of interests The authors declare that they have no known competing financial interests or personal relationships that could have appeared to influence the work reported in this paper.

References

- An J et al (2021) A shaking table-based experimental study of seismic response of shield-enlarge-dig type's underground subway station in liquefiable ground. *Soil Dyn Earthq Eng* 147:1–26. <https://doi.org/10.1016/j.soildyn.2021.106621>
- Bao X et al (2017) Numerical analysis on the seismic behavior of a large metro subway tunnel in liquefiable ground. *Tunn Undergr Space Technol* 66:91–106. <https://doi.org/10.1016/j.tust.2017.04.005>
- Beatty M, Byrne P (1998) An effective stress model for predicting liquefaction behaviour of sand. *Geotech Earthq Eng Soild Dyn ASCE Geotech Spec Pub* 75:766–777
- Beatty M, Byrne P (2011) Ubsand constitutive model. Itasca UDM website 904aR
- Bhattacharya S, Madabhushi S, Bolton M (2004) An alternative mechanism of pile failure in liquefiable deposits during earthquakes. *Geotechnique* 54(3):203–213
- Bolton M (1986) The strength and dilatancy of sands. *Géotechnique* 36(1):65–78
- Finn W, Fujita N (2002) Piles in liquefiable soils: seismic analysis and design issues. *Soil Dyn Earthq Eng* 22:731–742
- Hansen J (1970) A revised and extended formula for bearing capacity. Bulletin 28 Danish Geotechnical Institute Copenhagen
- Haque F (2023) Numerically liquefaction analysis of tunnel-sand pile interaction (TSPI) under seismic excitation. *Geomech Tunnell* 16(2):193–204. <https://doi.org/10.1002/geot.202200062>
- Hossain M, Ansary M (2018) Development of a portable travelling pluviator device and its performance to prepare uniform sand specimens. *Innov Infrastruct Solut* 3(1):1–12
- Huded P, Dash S, Bhattacharya S (2022) Buckling analysis of pile foundation in liquefiable soil deposit with sandwiched non-liquefiable layer. *Soil Dyn Earthq Eng* 154:1–13
- Hussein A, Naggar M (2021) Seismic axial behaviour of pile groups in non-liquefiable and liquefiable soils. *Soil Dyn Earthq Eng* 149:1–18
- Iai S (1989) Similitude for shaking table tests on soil-structure-fluid model in 1g gravitational field. *Soils Found* 29(1):105–118
- Liyanapathirana D, Poulos H (2002) A numerical model for dynamic soil liquefaction analysis. *Soil Dyn Earthq Eng* 22:1007–1015
- Maheshwari B, Nath U, Ramasamy G (2008) Influence of liquefaction on pile-soil interaction in vertical vibration. *ISIT J Earthq Technol* 45(1–2):1–12
- Makra A (2013) Evaluation of the UBC3D-PLM constitutive model for prediction of earthquake induced liquefaction on embankment dams. Delft University of Technology. <http://resolver.tudelft.nl/uuid:dfd7b8e4-8664-4026-bd3f-93749b72bfc8>
- Orang M et al (2021) An experimental evaluation of helical piles as a liquefaction-induced building settlement mitigation measure. *Soil Dyn Earthq Eng* 151:1–17
- Petalas A, Galavi V (2012) Plaxis liquefaction model ubc3d-plm. PLAXIS knowledge base
- Plaxis (2020) Material models manual. Bentley
- Puebla H, Byrne M, Phillips P (1997) Analysis of canlex liquefaction embankments prototype and centrifuge models. *Can Geotech J* 34:641–657
- Sahare A, Ueda K, Uzuoka R (2022) Influence of the sloping ground conditions and the subsequent shaking events on the pile group response subjected to kinematic interactions for a liquefiable sloping ground. *Soil Dyn Earthq Eng* 152:1–26
- Schadlich B, Schweiger H (2014) A new constitutive model for shotcrete. *Numerical Methods in Geotechnical Engineering*, pp 103–108
- Tang L et al (2021) Estimation of the critical buckling load of pile foundations during soil liquefaction. *Soil Dyn Earthq Eng* 146:1–11
- Taylor E, Madabhushi S (2020) Remediation of liquefaction-induced floatation of non-circular tunnels. *Tunn Undergr Space Technol* 98:1–8
- Tsegaye A (2010) Plaxis liquefaction model. Plaxis knowledge base
- Wang R et al (2022) Influence of vertical ground motion on the seismic response of underground structures and

- underground-aboveground structure systems in liquefiable ground. *Tunn Undergr Space Technol* 122:1–12. <https://doi.org/10.1016/j.tust.2021.104351>
- Yue F et al (2021) Shaking table test and numerical simulation on seismic performance of prefabricated corrugated steel utility tunnels on liquefiable ground. *Soil Dyn Earthq Eng* 141:1–18
- Zhao K et al (2020) Stability of immersed tunnel in liquefiable seabed under wave loadings. *Tunn Undergr Space Technol* 102:1–13
- Zhao K et al (2021) Seismic response of immersed tunnel in liquefiable seabed considering ocean environmental loads. *Tunn Undergr Space Technol* 115:1–14

Publisher's Note Springer Nature remains neutral with regard to jurisdictional claims in published maps and institutional affiliations.

Springer Nature or its licensor (e.g. a society or other partner) holds exclusive rights to this article under a publishing agreement with the author(s) or other rightsholder(s); author self-archiving of the accepted manuscript version of this article is solely governed by the terms of such publishing agreement and applicable law.